Numerische Mathematik (2020) 144:527–551
https://doi.org/10.1007/s00211-019-01099-7

Numerische Mathematik

Surface Crouzeix–Raviart element for the Laplace–Beltrami equation

Hailong Guo[1]

Received: 17 December 2018 / Revised: 7 October 2019 / Published online: 9 January 2020

Abstract
In this paper, we are concerned with the nonconforming finite element discretization of geometric partial differential equations. We construct a surface Crouzeix–Raviart element on the linear approximated surface, analogous to a flat surface. The optimal convergence theory for the new nonconforming surface finite element method is developed even though the geometric error exists. By taking an intrinsic viewpoint of manifolds, we introduce a new superconvergent gradient recovery method for the surface Crouzeix–Raviart element using only the information of discretized surface. The potential of serving as an asymptotically exact a posteriori error estimator is also exploited. A series of benchmark numerical examples are presented to validate the theoretical results and numerically demonstrate the superconvergence of the gradient recovery method.

Mathematics Subject Classification Primary 65N30; Secondary 45N08

1 Introduction

Numerical methods for approximating partial differential equations (PDEs) with solutions defined on surfaces are of growing interests over the last decades. Since the pioneer work of Dziuk [28], there is tremendous development on finite element methods [2,8,9,15,19,22–24,29,32,34,36,40,41]. Fluid equations on manifolds have many important applications in fluidic biomembranes [3,6], computer graphics [30,37], and geophysics [42,46]. Typically, numerical simulation of surface Stokes or Navier-Stokes equations is unavoidable. In the literature, there are several works on them, for example, see [7,31,39,43,44]. It is well known that the standard linear surface ele-

This work was partially supported by Andrew Sisson Fund of the University of Melbourne.

✉ Hailong Guo
hailong.guo@unimelb.edu.au

[1] School of Mathematics and Statistics, The University of Melbourne, Parkville, VIC 3010, Australia

ment is not a stable pair for surface Stokes equations [14]. It could be fixed by adding a stabilizing term [39,44] or using Taylor–Hood element [31].

In the planar domain case, a simple way to handle this difficulty is to use the Crouzeix–Raviart element. The Crouzeix–Raviart element was firstly proposed by Crouzeix and Raviart [20] to solve a steady Stokes equation. Different from the Courant element, such element is only continuous at edge centers of a triangulation. In that sense, it is a nonconforming element. In addition to being used to construct a simple stable finite element pair for Stoke problems, the method was also proven to be locking free for Lame problems [13]. It can be viewed as a universal element for solids, fluids, and electromagnetic, see the recent review paper [11] and the references therein.

Our first purpose is to extend this exotic nonconforming element to a surface setting. Compared to the counterpart in the flat space, there is an additional geometric error due to the discretization of the surface. One of the main difficulties is to estimate the nonconforming consistency error. The key ingredient of this step is to conduct all the error analysis on the discretized surface instead of on the exact surface. It should be pointed out that, in general, two triangles sharing a common edge are not on the same plane. The standard argument [10,18] for nonconforming finite element method cannot be applied directly and the nonconforming consistency error is coupled together with the geometric error. By using a delicate argument, we show that the geometric error has no impact on the overall convergence results.

The second purpose of this paper is to propose a superconvergent post-processing technique for the surface Crouzeix–Raviart element. On the planar domain case, there are several post-processing techniques [16,33] for the Crouzeix–Raviart element. In particular, Guo and Zhang employed a local least-squares fitting procedure at every edge center to generate a more accurate approximate gradient. The most straightforward way of generalizing such idea to a surface setting is to project a local patch on a discretized surface onto its tangent plane as in [47]. However, there are two barriers to the surface Crouzeix–Raviart element: first, it requires the exact normal vectors; second, it requires the edge centers located on the exact surface. Those two difficulties can be alleviated by going back to the original definition of the surface derivative as in [26]. Instead of using the tangential gradient to define the surface gradient, we look at the intrinsic definition of the surface gradient. In the intrinsic sense, we can compute the surface gradient in term of the metric tensor of the surface. Also, we note that a manifold is locally differential homeomorphism to a Euclidean space. By introducing a local parametric mapping, we can map a parametric domain in Euclidean space to a local port of the manifold. The metric tensor of the manifold can be computed by using the Jacobi matrix of the parametric mapping. A distinctive feature of computing surface gradient in this way is the independence of the choice of the local parametric mapping and the local parametric domain. To recover the surface gradient, it suffices to reconstruct the gradient of a local function defined on the local parametric domain and the local parametric mapping. Since both the local function and local parametric mapping are defined on the Euclidean space, we can approximate them by polynomials. In specific, we can use a quadratic polynomial to locally approximate the local function and use a quadratic surface to locally approximate the local manifold. The reconstructed surface gradient is obtained by taking the gradient of the fitted least-squares polynomials and putting them in the intrinsic definition. In other words, we

firstly adopt a least-squares procedure to recover the local parametric mapping and then employ another least-squares fitting on the parameter domain. The proposed surface gradient recovery method only uses the information of the discretized surface and never requires any information about the exact surface. Furthermore, it doesn't require the vertices of the discretized surface to be on the exact surface. The recovered surface gradient is numerically proven to be superconvergent to the exact surface gradient. Based on the gradient recovery method, we introduce a recovery-type a posteriori error estimator for the surface Crouzeix–Raviart element. We numerically demonstrate that the recovery-type a posteriori error estimator is asymptotically exact.

The rest of the paper is organized as follows. In Sect. 2, we give a brief introduction to some preliminary knowledge on the tangential derivative and an exemplary model problem. In Sect. 3, we introduce the discretized surface and present the surface Crouzeix–Raviart element. Section 4 is devoted to the analysis of discrete energy error and L^2 error on the discretized surface. In Sect. 5, we propose a superconvergent post-processing technique. A series of benchmark numerical examples are presented to support our theoretical finding in Sect. 6. Some conclusions are drawn in Sect. 7.

2 Preliminary

2.1 Notation

In the paper, we shall consider Γ is an oriented, connected, and C^∞ smooth regular surface in $\mathbb{R}^3$ without boundary. The sign distance function of Γ is denoted by $d(x)$. Let ∇ be the standard gradient operator in $\mathbb{R}^3$. Then the unit outer normal vector of Γ is $n(x) = \nabla d(x)$ and the Weingarten map is $\mathbf{H}(x) = \nabla n(x) = \nabla^2 d(x)$.

Let $U = \{x \in \mathbb{R}^3 : \text{dist}(x, \Gamma) \leq \delta\}$ be a strip neighborhood around Γ with distance δ where $\text{dist}(x, \Gamma)$ is the Euclidean distance between x and Γ. Assume δ is small enough such that there exists a unique projection $p(x) : U \to \Gamma$ in the form of

$$p(x) = x - d(x)n(p(x)). \tag{2.1}$$

Let $P = Id - n \otimes n$ be the tangential projection operator where $\otimes$ is the tensor product. The tangential gradient of a scalar function v on Γ is defined to be

$$\nabla_\Gamma u = P\nabla u = \nabla u - (\nabla u \cdot n)n. \tag{2.2}$$

For a vector field $w \in \mathbb{R}^3$, the tangential divergence of w is

$$\text{div}_\Gamma w = \nabla_\Gamma \cdot w = \nabla \cdot w - n^t \nabla w n \tag{2.3}$$

The Laplace–Beltrami operator Δ_Γ is just the tangential divergence of the tangential gradient, i.e.

$$\Delta_\Gamma v = \text{div}_\Gamma \nabla_\Gamma v = \Delta v - (\nabla v \cdot n)(\nabla \cdot n) - n^t \nabla^2 v n. \tag{2.4}$$

Let $\alpha = (\alpha_1, \alpha_2, \alpha_3)$ be the 3-index and $|\alpha| = \sum_{i=1}^{3} \alpha_i$ with α_i being a nonnegative integer. Let D_Γ^α be the $|\alpha|$-th order tangential derivative. Assume ω is a subset of Γ and m is a nonnegative integer. The Sobolev space $H^m(\omega)$ on ω [48] is defined as

$$H^m(\omega) = \left\{ v \in L^2(\omega) | D_\Gamma^\alpha v \in L^2(\omega), |\alpha| \leq m \right\}, \tag{2.5}$$

equipped with norm

$$\|v\|_{H^m(\omega)} = \left(\sum_{\alpha \leq m} \|D_\Gamma^\alpha v\|_{L^2(\omega)}^2 \right)^{1/2}, \tag{2.6}$$

and semi-norm

$$|v|_{H^m(\omega)} = \left(\sum_{\alpha = m} \|D_\Gamma^\alpha v\|_{L^2(\omega)}^2 \right)^{1/2}. \tag{2.7}$$

Throughout this paper, let $x \lesssim y$ be the shorthand of $x \leq Cy$ where the letter C denotes a generic constant which is independent of h and may not be the same at each occurrence.

2.2 Model problem

In this paper, we shall consider the following model Laplace–Beltrami equation

$$-\Delta_\Gamma u + u = f, \tag{2.8}$$

for a given $f \in L^2(\Gamma)$.

The variational formulation of (2.8) is to find $u \in H^1(\Gamma)$ such that

$$a(u, v) = \ell(v), \quad \forall v \in H^1(\Gamma) \tag{2.9}$$

where

$$a(w, v) = (\nabla_\Gamma w, \nabla_\Gamma v) + (w, v), \tag{2.10}$$

and

$$\ell(v) = (f, w), \tag{2.11}$$

with $(\cdot, \cdot)$ being the standard L^2 inner product on Γ. The Lax–Miligram theorem implies (2.9) has a unique solution and we have the following regularity [4]

$$\|u\|_{H^2(\Gamma)} \lesssim \|f\|_{L^2(\Gamma)}. \tag{2.12}$$

3 The nonconforming finite element method

3.1 Approximate surface

Suppose Γ_h is a polyhedral approximation of Γ with planar triangular surface. Let $\mathcal{T}_h$ be the associated triangulation of Γ_h and $h = \max_{T\in\mathcal{T}_h} \mathrm{diam}(T)$ be its maximum diameter. Furthermore, we assume the mesh $\mathcal{T}_h$ is shape regular and quasi-uniform triangulation [10,12,18] and all vertices lie on Γ. Let $\mathcal{E}_h$ be the set of all edges of triangular faces in $\mathcal{T}_h$. For any edge $E \in \mathcal{E}_h$, let m_E be the middle point of edge E. The set of all edge centers of $\mathcal{T}_h$ is denoted by $\mathcal{M}_h$. For any $T \in \mathcal{T}_h$, let n_h be the unit outer normal vector to Γ_h on T. The projection onto the tangent space of Γ_h can be defined as

$$P_h = Id - n_h \otimes n_h. \tag{3.1}$$

Similarly, for any scalar function v on Γ_h, we can define its tangential gradient as

$$\nabla_{\Gamma_h} v = P_h \nabla v, \tag{3.2}$$

and the Laplace–Beltrami operator on Γ_h as

$$\Delta_{\Gamma_h} v = \nabla_{\Gamma_h} \cdot \nabla_{\Gamma_h} v_h \tag{3.3}$$

Recall that $p(x)$ is a projection from U to Γ. For any $T \in \mathcal{T}_h$, let $T^l = p(T)$ be the curved triangular face on Γ. Denote the set of all curved triangular faces by $\mathcal{T}_h^l$, i.e. $\mathcal{T}_h^l = \left\{T^l : T \in \mathcal{T}_h\right\}$. Then $\mathcal{T}_h^l$ forms a conforming triangulation of Γ such that

$$\Gamma = \bigcup_{T^l\in\mathcal{T}_h^l} T^l. \tag{3.4}$$

For any edge $E \in \mathcal{E}_h$, there exists two triangles T^+ and T^- such that $E = \partial T^+ \cap \partial T^-$. The projection onto T^+ and T^- are denoted by P_h^+ and P_h^-. Also, we use the notation $\nabla_{\Gamma_h}^+ = P_h^+ \nabla$ to denote the tangential gradient in T^+. Similar notation is adopted in T^-. The conormal of E to T^+, which is denoted by n_E^+, is the unit outward vector of E in the tangent plane of T^+. Similarly, let n_E^- be the conormal of E to T^-. Analogously, on the curved edge $E^l = p(E)$, we denote its conormals by $n_{E^l}^{\pm}$. Note that $n_{E^l}^+ = -n_{E^l}^-$. The unit outer normals of Γ_h on T^+ and T^- are denoted by n_h^+ and n_h^-, respectively. Then it easy to see that $n_h^+ \perp n_E^+$ and $n_h^- \perp n_E^-$. We define the jump of a function v_h across E by

$$[\![v]\!] = \lim_{s\to 0+} \left(v(x - sn_E^+) - v(x - sn_E^-)\right). \tag{3.5}$$

3.2 The surface Crouzeix–Raviart finite element method

The surface Crouzeix–Raviart finite element space on $\mathcal{T}_h$ is defined to be

$$V_h = \left\{ v_h \in L^2(\Gamma_h) : v_h|_T \in \mathbb{P}^1(T) \text{ and } v_h \text{ is continuous at } \mathcal{M}_h \right\}, \tag{3.6}$$

where $\mathbb{P}_1(T)$ is the set of linear polynomials on T. By the definition of jump of a function in (3.5) and the midpoint rule, a piecewise linear function v is in V_h if and only if

$$\int_E [\![v]\!] d\sigma_h = 0. \tag{3.7}$$

To simplify the notation, we firstly define a discrete bilinear form $a_h(\cdot,\cdot)$ on $V_h \times V_h$ as

$$a_h(w_v, v_h) = \sum_{T\in\mathcal{T}_h} \int_T \nabla_{\Gamma_h} w_h \cdot \nabla_{\Gamma_h} w_h ds_h + (w_h, v_h)_{\Gamma_h}, \tag{3.8}$$

and a discrete linear functional $\ell_h(\cdot)$ on V_h as

$$\ell_h(v_h) = (f \circ p, v_h)_{\Gamma_h}. \tag{3.9}$$

where $(\cdot,\cdot)_{\Gamma_h}$ is the standard L^2 inner product of $L^2(\Gamma_h)$. Then the surface Crouzeix–Raviart finite element discretization of the model problem (2.8) reads as: find $u_h \in V_h$ such that

$$a_h(u_h, v_h) = \ell_h(v_h), \quad \forall v_h \in V_h. \tag{3.10}$$

We define an broken H_1 semi-norm on V_h as

$$|v_h|^2_{H^1(\Gamma_h;\mathcal{T}_h)} = \sum_{T\in\mathcal{T}_h} \|\nabla_{\Gamma_h} v_h\|^2_{L^2(T)}. \tag{3.11}$$

The corresponding discrete energy norm is given by

$$\|v\|_h^2 = |v_h|^2_{H^1(\Gamma_h;\mathcal{T}_h)} + \|v_h\|^2_{L^2(\Gamma_h)} = a_h(v_h, v_h). \tag{3.12}$$

Then, it is easy to show the following Lemma:

Lemma 3.1 *$\|v\|_h$ is a norm on V_h. The Lax–Milgram theorem implies the discrete variational problem (3.10) admits a unique solution.*

4 A priori error estimates

4.1 Lift and extension functions

To compare the error between the exact solution u defined on Γ and the finite element solution u_h defined on Γ_h, we need to establish connections between the functions defined on Γ and Γ_h.

Following the notation as in [15], for a function v defined on Γ, we extend it to U and define the extension v^e by

$$v^e(x) = v(p(x)), \quad \forall x \in U. \tag{4.1}$$

Similarly, for a function v_h defined on Γ_h, we define the lift of v_h onto Γ by

$$v^l(x) = v(\xi(x)), \quad \forall x \in \Gamma, \tag{4.2}$$

where $\xi(x)$ is the unique solution of

$$x = p(\xi) = \xi - d(\xi)n(x). \tag{4.3}$$

Then we build the relationship in gradients of extensions and lifts. For such purpose, we introduce the matrix $B = P(x) - d(x)H(x)$. It is easy to check that $B = PB = BP = PBP$. The following relationship can be found in [15,24,34]

$$\nabla_{\Gamma_h} v^e = P_h B (\nabla_\Gamma v)^e. \tag{4.4}$$

Let ds and ds_h be the surface measures of Γ and Γ_h. For any $x \in \Gamma_h$, [24] shows that there exists μ_h such that $ds \circ p(x) = \mu_h(x) ds_h(x)$ with

$$\mu_h(x) = (1 - d(x)k_1(x))(1 - d(x)k_2(x))n \cdot n_h. \tag{4.5}$$

Throughout the paper, we assume that $\Gamma_h \subset U$. In the following, we collect some geometric approximation results which will be used in our proof:

Lemma 4.1 *Suppose $\Gamma_h \subset U$ is a polyhedral approximation of Γ. Assume the mesh size h is small enough. Then the following error estimates hold:*

$$\|d\|_{L^\infty(T)} \lesssim h^2, \tag{4.6}$$

$$\|1 - \mu_h\|_{L^\infty(T)} \lesssim h^2, \tag{4.7}$$

$$\|n - n_h\|_{L^\infty(T)} \lesssim h, \tag{4.8}$$

$$\|P - P_h\|_{L^\infty(T)} \lesssim h, \tag{4.9}$$

$$\|n_{E^l}^{+/-} - P n_E^{+/-}\|_{L^\infty(T)} \lesssim h^2, \tag{4.10}$$

$$\|\Delta_{\Gamma_h} u^e - (\Delta_\Gamma u)^e\|_{L^2(T)} \lesssim h \|u\|_{H^2(T^l)}. \tag{4.11}$$

Proof The inequalities (4.6)–(4.9) can be proved using the standard linear interpolation theory. Their proofs can be found in [28]. The last two estimates were proven in [34].

Remark 4.1 For the planar domain case, it is well known that $n_E^+ = -n_E^-$ and hence $|n_E^+ + n_E^-| = 0$. But this relationship does not hold any more in the surface setting.

To connect the function defined on the exact surface and its extension on the discrete surface, we need the following norm equivalence theorem whose proof can be found in [28].

Lemma 4.2 *Let $T \in \mathcal{T}_h$. If $v \in H^2(T)$, then the following results hold:*

$$\|v^l\|_{L^2(T^l)} \lesssim \|v\|_{L^2(T)} \lesssim \|v^l\|_{L^2(T^l)}, \tag{4.12}$$

$$|v^l|_{H^1(T^l)} \lesssim |v|_{H^1(T)} \lesssim |v^l|_{H^1(T^l)}, \tag{4.13}$$

$$|v|_{H^2(T)} \lesssim \|v^l\|_{H^2(T^l)}, \tag{4.14}$$

$$|v^l|_{H^2(T^l)} \lesssim \|v\|_{H^2(T)}. \tag{4.15}$$

Also, we need the following norm equivalence results for function defined on the edge of an element [15,28].

Lemma 4.3 *Let $E \in \mathcal{E}_h$. If $v \in H^1(E)$, then the following results hold:*

$$\|v^l\|_{L^2(E^l)} \lesssim \|v\|_{L^2(E)} \lesssim \|v^l\|_{L^2(E^l)}, \tag{4.16}$$

$$|v^l|_{H^1(E^l)} \lesssim |v|_{H^1(E)} \lesssim |v^l|_{H^1(E^l)}. \tag{4.17}$$

4.2 The nonconforming interpolation

For any $T \in \mathcal{T}_h$, let $\mathcal{E}_T$ be the set of three edges of T. We define the local interpolation operator $\Pi_T : H^1(T) \to \mathbb{P}_1(T)$ by

$$(\Pi_T v)(m_E) = \frac{1}{|E|}\int_E v d\sigma_h, \quad \forall v \in H^1(T),\ E \in \mathcal{E}_T, \tag{4.18}$$

where $|E|$ is the length of E. By the midpoint rule, we can show that

$$\int_E (\Pi_T v) d\sigma_h = \int_E v d\sigma_h, \quad E \in \mathcal{E}_T. \tag{4.19}$$

Let h_T be the diameter of T. Then the following local interpolation error estimate holds [11,20]

$$\|v - \Pi v\|_{L^2(T)} + h_T |v - \Pi v|_{H^1(T)} \lesssim h_T^2 |v|_{H^2(T)}, \tag{4.20}$$

for any $v \in H^2(T)$. The global interpolation operator $\Pi_h : H^1(\Gamma_h) \to V_h$ is defined by

$$(\Pi_h v)|_T = \Pi_T v, \quad \forall T \in \mathcal{T}_h. \tag{4.21}$$

The local interpolation error estimate (4.20) implies the following global interpolation error estimate

$$\|v - \Pi_h v\|_{L^2(\Gamma_h)} + h|v - \Pi_h v|_{H^1(\Gamma_h;\mathcal{T}_h)} \lesssim h^2 |v|_{H^2(\Gamma_h)}, \tag{4.22}$$

In particular, let $v = u^e$. Then we have

$$\inf_{v_h \in V_h} \|u^e - v_h\|_h \le |u^e - \Pi_h u^e|_{H^1(\Gamma_h;\mathcal{T}_h)} + \|u^e - \Pi_h u^e\|_{L^2(\Gamma_h)} \lesssim h|u^e|_{H^2(\Gamma_h)}. \tag{4.23}$$

4.3 Energy error estimate

In this subsection, we shall establish the error bound in the discrete energy error. Our main tool of the error estimation is the second Strang Lemma [10,12,18].

Lemma 4.4 (The second Strang Lemma) *Suppose u is the exact solution of (2.9) and u_h is the finite element solution of (3.10). Then we obtain that*

$$||u^e - u_h||_h \lesssim \inf_{v_h \in V_h} \|u^e - v_h\|_h + \sup_{w_h \in V_h} \frac{|a_h(u^e, w_h) - (f^e, w_h)|}{\|w_h\|_h}. \tag{4.24}$$

Remark 4.2 The first term in (4.24) is also referred to the approximation error and the second term is referred to the nonconforming consistency error. Different from the planar domain case, the second term also involves the geometric error in addition to the classical nonconforming consistency error. We measure the error using the discrete energy norm on the discretized surface and this is the key part to bound the nonconforming consistency error.

We prepare the energy error estimation with some geometric error estimates. In specific, we start with the following Lemma:

Lemma 4.5 *Let u be the solution of (2.9) and u^e be its extension to U defined by (4.1). Then we have the following error estimates hold*

$$|(u, w_h^l) - (u^e, w_h)_{\Gamma_h}| \lesssim h^2 \|u\|_{L^2(\Gamma)} \|w_h\|_{L^2(\Gamma_h)}, \tag{4.25}$$

$$|(f, w_h^l) - (f^e, w_h)_{\Gamma_h}| \lesssim h^2 \|f\|_{L^2(\Gamma)} \|w_h\|_{L^2(\Gamma_h)}, \tag{4.26}$$

for any $w_h \in V_h$.

Proof We only prove (4.26) and (4.25) can be proved similarly. Applying the change of variable, we have

$$|(f, w_h^l) - (f^e, w_h)_{\Gamma_h}| \lesssim |((\mu_h - 1) f^e, w_h)_{\Gamma_h} \lesssim h^2 \|f^e\|_{L^2(\Gamma_h)} \|w_h\|_{L^2(\Gamma_h)},$$

where we have used the error estimate (4.7). □

Next, we are going to establish the error estimation involving the integral of the difference of two conformal vectors along an edge.

Lemma 4.6 *Let u be the solution of (2.9) and u^e be its extension to U defined by (4.1). Then the following error estimate holds*

$$\sum_{E \in \mathcal{E}_h} \int_E \left(n_E^+ \cdot \nabla_{\Gamma_h}^+ u^e + n_E^- \cdot \nabla_{\Gamma_h}^- u^e \right)^2 d\sigma_h \leq h^3 \|u\|_{H^2(\Gamma)}^2. \tag{4.27}$$

Proof Using the triangle inequality and (4.4), we have

$$\begin{aligned}
&\int_E \left(n_E^+ \cdot \nabla_{\Gamma_h}^+ u^e + n_E^- \cdot \nabla_{\Gamma_h}^- u^e\right)^2 d\sigma_h \\
&= \int_E \left(n_E^+ \cdot P_h^+ B(\nabla_\Gamma u)^e + n_E^- \cdot P_h^- B(\nabla_\Gamma u)^e\right)^2 d\sigma_h \\
&= \int_E \left(P n_E^+ \cdot B(\nabla_\Gamma u)^e + P n_E^- \cdot B(\nabla_\Gamma u)^e\right)^2 d\sigma_h \\
&\lesssim \int_E \left((P n_E^+ - n_{E^l}^+) \cdot B(\nabla_\Gamma u)^e\right)^2 d\sigma_h \\
&\quad + \int_E \left((n_{E^l}^- - P n_E^-) \cdot B(\nabla_\Gamma u)^e\right)^2 d\sigma_h \\
&\lesssim h^4 \int_E \left|(\nabla_\Gamma u)^e\right|^2 d\sigma_h \\
&\lesssim h^4 \int_{E^l} |\nabla_\Gamma u|^2 \, d\sigma,
\end{aligned} \tag{4.28}$$

where we have used (4.10) in the second inequality and norm equivalence (4.17) in the last inequality.

Summing over over all $E \in \mathcal{E}_h$ and applying the trace inequality, we have

$$\begin{aligned}
&\sum_{E\in\mathcal{E}_h} \int_E \left(n_E^+ \cdot \nabla_{\Gamma_h}^+ u^e + n_E^- \cdot \nabla_{\Gamma_h}^- u^e\right)^2 d\sigma_h \\
&\lesssim h^4 \sum_{E\in\mathcal{E}_h} \int_{E^l} |\nabla_\Gamma u|^2 \, d\sigma \\
&\lesssim h^4 \sum_{T\in\mathcal{T}_h} \int_{\partial T^l} |\nabla_\Gamma u|^2 \, d\sigma \\
&\lesssim h^4 \sum_{T\in\mathcal{T}_h} \left(h^{-1} \|\nabla_\Gamma u\|_{L^2(T^l)}^2 + h |\nabla_\Gamma u|_{H^1(T^l)}^2\right) \\
&\lesssim h^3 \|u\|_{H^2(\Gamma)}^2,
\end{aligned} \tag{4.29}$$

which completes our proof. □

In the next Lemma, we shall estimate the main term in the nonconforming consistency error by using an argument analogous to the Crouzeix–Raviart element in planar domain [10].

Lemma 4.7 *Let u be the solution of (2.9) and u^e be its extension to U defined by (4.1). Then the following error estimate holds*

$$\sum_{E\in\mathcal{E}_h} \int_E n_E^+ \cdot \nabla_{\Gamma_h}^+ u^e [\![w_h]\!] d\sigma_h \lesssim h |u^e|_{H^2(\Gamma)} |w_h|_{H^1(\Gamma_h;\mathcal{T}_h)}. \tag{4.30}$$

for any $w_h \in V_h$.

Proof Let $\Pi_E^0 w_h = \frac{1}{|E|}\int_E w_h d\sigma_h$. Using the fact $[\![\Pi_E^0 w_h]\!] = 0$ and the Cauchy Schwartz inequality, we have

$$\begin{aligned}
&\sum_{E\in\mathcal{E}_h}\int_E n_E^+ \cdot \nabla_{\Gamma_h}^+ u^e [\![w_h]\!] d\sigma_h \\
&= \sum_{E\in\mathcal{E}_h}\int_E n_E^+ \cdot \nabla_{\Gamma_h}^+ u^e [\![w_h - \Pi_E^0 w_h]\!] d\sigma_h \\
&= \sum_{E\in\mathcal{E}_h}\int_E n_E^+ \cdot \nabla_{\Gamma_h}^+ (u^e - \Pi_h u^e) [\![w_h - \Pi_E^0 w_h]\!] d\sigma_h \\
&= \sum_{E\in\mathcal{E}_h}\left(\int_E |\nabla_{\Gamma_h}^+ (u^e - \Pi_h u^e)|^2 d\sigma_h\right)^{1/2}\left(\int_E [\![w_h - \Pi_E^0 w_h]\!]^2 d\sigma_h\right)^{1/2}. \qquad (4.31)
\end{aligned}$$

Arguing similarly using the trace inequality, the Poincare's inequality and (4.20) as in planar domain [10], we obtain

$$\int_E |\nabla_{\Gamma_h}^+ (u^e - \Pi_h u^e)|^2 d\sigma_h \lesssim h|u|^2_{H^2(T^+)}, \qquad (4.32)$$

$$\int_E [\![w_h - \Pi_E^0 w_h]\!]^2 d\sigma_h \lesssim h\left(|w_h|^2_{H^1(T^+)} + |w_h|^2_{H^1(T^-)}\right). \qquad (4.33)$$

Combining the estimates (4.31)–(4.33) gives (4.30). □

Now, we are prepared to prove the nonconforming consistency error:

Lemma 4.8 *Let u be the solution of (2.9) and u^e be its extension to U defined by (4.1). Then the following error estimate holds*

$$|a_h(u^e, w_h) - (f^e, w_h)_{\Gamma_h}| \lesssim h\|u\|_{H^2(\Gamma)}\|w_h\|_h. \qquad (4.34)$$

for any $w_h \in V_h$.

Proof For any $w_h \in V_h$, we notice that

$$a_h(u^e, w_h) - (f^e, w_h)_{\Gamma_h} = [a_h(u^e, w_h) - (f, w_h^l)] + [(f, w_h^l) - (f^e, w_h)_{\Gamma_h}]. \qquad (4.35)$$

Using (4.26), the second term can be estimated as

$$|(f, w_h^l) - (f^e, w_h)_{\Gamma_h}| \lesssim h^2\|f\|_{L^2(\Gamma)}\|w_h\|_{L^2(\Gamma_h)} \lesssim h^2\|u\|_{H^2(\Gamma)}\|w_h\|_h. \qquad (4.36)$$

where we used the fact $f = -\Delta_\Gamma u + u$.

To estimate the first term, we apply the Green's formula and we obtain that

$$
\begin{aligned}
&a_h(u^e, w_h) - (f, w_h^l) \\
&= \sum_{E\in\mathcal{E}_h}\int_E \left(n_E^+ \cdot \nabla_{\Gamma_h}^+ u^e w_h^+ + n_E^- \cdot \nabla_{\Gamma_h}^- u^e w_h^-\right) d\sigma_h \\
&\quad - \sum_{T\in\mathcal{T}_h} (\Delta_{\Gamma_h} u^e, w_h)_T - (\Delta_\Gamma u, w_h^l) + (u^e, w_h)_{\Gamma_h} - (u, w_h^l) \\
&= \sum_{E\in\mathcal{E}_h}\int_E \left(n_E^+ \cdot \nabla_{\Gamma_h}^+ u^e + n_E^- \cdot \nabla_{\Gamma_h}^- u^e\right) w_h^- d\sigma_h + \left[(u^e, w_h)_{\Gamma_h} - (u, w_h^l)\right] \\
&\quad \sum_{E\in\mathcal{E}_h}\int_E n_E^+ \cdot \nabla_{\Gamma_h}^+ u^e [\![w_h]\!] \sigma_h + \left[(\Delta_\Gamma u, w_h^l) - \sum_{T\in\mathcal{T}_h} (\Delta_{\Gamma_h} u^e, w_h)_T\right] \\
&= I_1 + I_2 + I_3 + I_4. \qquad (4.37)
\end{aligned}
$$

To estimate I_1, we use Lemma 4.6, the Cauchy–Schwartz inequality, and the trace inequality to get

$$
\begin{aligned}
|I_1| &\le \left(\sum_{E\in\mathcal{E}_h}\int_E \left(n_E^+ \cdot \nabla_{\Gamma_h}^+ u^e + n_E^- \cdot \nabla_{\Gamma_h}^- u^e\right)^2 d\sigma_h\right)^{1/2} \left(\sum_{E\in\mathcal{E}_h}\int_E (w_h^-)^2 d\sigma_h\right)^{1/2} \\
&\lesssim h^{3/2}\|u\|_{H^2(\Gamma)} \left(h^{-1/2}\|w_h\|_{L^2(\Gamma_h)} + h^{1/2}|w_h|_{H^1(\Gamma_h;\mathcal{T}_h)}\right) \\
&\lesssim h\|u\|_{H^2(\Gamma)}\|w_h\|_h.
\end{aligned}
$$

According to Lemmas 4.5 and 4.7, we have

$$
|I_2| + |I_3| \lesssim h\|u\|_{H^2(\Gamma)}\|w_h\|_h.
$$

Then, we estimate I_4. By the triangle inequality and the error estimate (4.11) and (4.9), we have

$$
\begin{aligned}
|I_4| &= |\sum_{T\in\mathcal{T}} (\Delta_\Gamma u, w_h^l)_{T^l} - \sum_{T\in\mathcal{T}_h} (\Delta_{\Gamma_h} u^e, w_h)_T| \\
&\le \sum_{T\in\mathcal{T}} \left|(\mu_h(\Delta_\Gamma u)^e, w_h^l)_T - (\Delta_{\Gamma_h} u^e, w_h)_T\right| \\
&\le \sum_{T\in\mathcal{T}} |((\mu_h - 1)(\Delta_\Gamma u)^e, w_h)_T| + \sum_{T\in\mathcal{T}} |((\Delta_\Gamma u)^e - \Delta_{\Gamma_h} u^e, w_h)_T| \\
&\lesssim h\|u\|_{H^2(\Gamma)}\|w_h\|_{L^2(\Gamma_h)}.
\end{aligned}
$$

Summing the above three error estimates, we complete the proof of (4.34). □

With all the previous preparations, we are now in a perfect position to prove the following energy error estimate

Theorem 4.9 *Let u be the solution of (2.9) and u^e be its extension to U defined by (4.1). Then we have the following error estimate*

$$\|u^e - u_h\|_h \lesssim h\|f\|_{L^2(\Gamma)}. \tag{4.38}$$

Proof Using Lemma 4.8 and the regularity estimate (2.12), we obtain that

$$\sup_{w_h \in V_h} \frac{|a_h(u^e, w_h) - \ell(w_h^l)|}{\|w_h\|_h} \lesssim h\|f\|_{L^2(\Gamma)}. \tag{4.39}$$

We complete our proof by combining the second Strang Lemma 4.4 and the estimates (4.23) and (4.39). □

4.4 L_2 error estimate

In this subsection, we shall establish a priori error estimate in L^2 norm using the Abuin–Nitsche's trick [10,12,18]. Let $g = u - u_h^l \in L^2(\Gamma)$. The dual problem is to find $\phi \in H^1(\Gamma)$ such that

$$a(v, \phi) = (v, g), \quad \forall v \in H^1(\Gamma). \tag{4.40}$$

Similarly, we have the following regularity result:

$$\|\phi\|_{H^2(\Gamma)} \leq \|g\|_{L^2(\Gamma)}. \tag{4.41}$$

The surface Crouzeix–Raviart element discretization of the dual problem is to find $\phi_h \in V_h$ such that

$$a_h(v_h, \phi_h) = (v_h, g^e), \quad \forall v_h \in V_h, \tag{4.42}$$

where $g^e = (u - u_h^l)^e = u^e - u_h$. By Theorem 4.9, we have the following energy error estimate for the dual problem

$$\|\phi^e - \phi_h\|_h \lesssim h\|g\|_{L^2(\Gamma)}. \tag{4.43}$$

We begin our L^2 error estimate with the following Lemma:

Lemma 4.10 *Let u be the solution of (2.9) and ϕ be the solution of the dual problem (4.40). Then we have the following error estimate*

$$a_h(u^e, \phi^e) - a(u, \phi) \lesssim h^2\|u\|_{H^2(\Gamma)}\|\phi\|_{H^2(\Gamma)}. \tag{4.44}$$

Proof (4.44) can be proved by using the same technique as in continuous linear surface finite element, see [28].

Then, we shall prove a lemma involving global interpolation Π_h.

Lemma 4.11 *Let u be the solution of (2.9) and ϕ be the solution of the dual problem (4.40). Then we have the following error estimate*

$$a_h(u^e, \phi^e - \Pi_h\phi^e) \lesssim h^2\|u\|_{H^2(\Gamma)}\|\phi\|_{H^2(\Gamma)}, \tag{4.45}$$

$$a_h(u^e - \Pi_h u^e, \phi^e) \lesssim h^2\|u\|_{H^2(\Gamma)}\|\phi\|_{H^2(\Gamma)}. \tag{4.46}$$

Proof We only give a proof of (4.45) and (4.46) can be proved similarly. To prove (4.45), we apply the integration by part formula and use (4.19) which gives

$$\begin{aligned} a_h(u^e, \phi^e - \Pi_h\phi^e) &= \sum_{T\in\mathcal{T}_h} (\nabla_{\Gamma_h} u^e, \nabla_{\Gamma_h}(\phi^e - \Pi_h\phi^e)) + (u^e, \phi^e - \Pi_h\phi^e) \\ &= -(\Delta_{\Gamma_h} u^e, \phi^e - \Pi_h\phi^e) + (u^e, \phi^e - \Pi_h\phi^e) \end{aligned}$$

Then (4.45) follows by using the Cauchy–Schwartz inequality, the interpolation error estimate (4.22), and the norm equivalence Lemma 4.2. □

Using the above Lemma, we can prove the following consistency error estimate:

Lemma 4.12 *Let u be the solution of (2.9) and ϕ be the solution of the dual problem (4.40). Then we have the following error estimate*

$$a_h(u^e, \phi^e - \phi_h) - ((f,\phi) - (f^e, \phi_h)_{\Gamma_h}) \lesssim h^2\|u\|_{H^2(\Gamma)}\|\phi\|_{H^2(\Gamma)}, \tag{4.47}$$

$$a_h(u^e - u_h, \phi^e) - ((u,g) - (u_h, g^e)_{\Gamma_h}) \lesssim h^2\|u\|_{H^2(\Gamma)}\|\phi\|_{H^2(\Gamma)}. \tag{4.48}$$

Proof To prove (4.47), we notice that

$$\begin{aligned} &a_h(u^e, \phi^e - \phi_h) - [(f,\phi) - (f^e, \phi_h)_{\Gamma_h}] \\ &\quad = [a_h(u^e, \Pi_h\phi^e - \phi_h) - (f^e, \Pi_h\phi^e - \phi_h)_{\Gamma_h}] + a_h(u^e, \phi^e - \Pi_h\phi^e) \\ &\qquad -[(f,\phi) - (f^e, \phi^e)_{\Gamma_h}] - (f^e, \phi^e - \Pi\phi^e)_{\Gamma_h} \\ &\quad = I_1 + I_2 + I_3 + I_4. \end{aligned}$$

We first estimate I_1. Using Lemma 4.8, we obtain

$$\begin{aligned} |I_1| &\lesssim h\|u\|_{H^2(\Gamma)}\|\Pi_h\phi^e - \phi_h\|_h \\ &\lesssim h\|u\|_{H^2(\Gamma)}(\|\Pi_h\phi^e - \phi^e\|_h + \|\phi^e - \phi_h\|_h) \\ &\lesssim h^2\|u\|_{H^2(\Gamma)}\|\phi\|_{H^2(\Gamma)}, \end{aligned}$$

where we have used the energy error estimate (4.38) in the second inequality.

According to Lemmas 4.11 and 4.5, we have

$$|I_2| + |I_3| \lesssim h^2\|f\|_{L^2(\Gamma)}\|g\|_{L^2(\Gamma)}.$$

To estimate I_4, we use the Cauchy–Schwartz inequality and (4.22) which yields that

$$|I_4| \le \|f^e\|_{L^2(\Gamma_h)}\|\phi^e - \Pi\phi^e\|_{L^2(\Gamma_h)} \lesssim h^2\|f\|_{L^2(\Gamma)}\|g\|_{L^2(\Gamma)}.$$

Summing all the above error estimates concludes the proof (4.47). The error estimate (4.48) can be proved in the same way. □

Now, we are ready to present our error estimate in L^2 norm.

Theorem 4.13 *Let u be the solution of (2.9) and u^e be its extension to U defined by (4.1). Then we have the following error estimate*

$$\|u^e - u_h\|_{L^2(\Gamma_h)} \leq h^2 \|f\|_{L^2(\Gamma)}. \tag{4.49}$$

Proof Using (2.9), (3.10), (4.40) and (4.42), we have

$$\begin{aligned}
&\|u^e - u_h\|^2_{L^2(\Gamma_h)} = (u^e - u_h, g^e)_{\Gamma_h} \\
&= (u^e, g^e)_{\Gamma_h} - (u, g) + (u, g) - (u_h, g^e) \\
&= (u^e, g^e)_{\Gamma_h} - (u, g) + a(u, \phi) - a_h(u_h, \phi_h) \\
&= [(u^e, g^e)_{\Gamma_h} - (u, g)] + [a(u, \phi) - a_h(u^e, \phi^e)] + [a_h(u^e, \phi^e) - a_h(u_h, \phi_h)] \\
&= [(u^e, g^e)_{\Gamma_h} - (u, g)] + [a(u, \phi) - a_h(u^e, \phi^e)] + a_h(u^e - u_h, \phi^e - \phi_h) \\
&\quad + a_h(u_h, \phi^e - \phi_h) + a_h(u^e - u_h, \phi_h) \\
&= [(u^e, g^e)_{\Gamma_h} - (u, g)] - [a(u, \phi) - a_h(u^e, \phi^e)] + a_h(u^e - u_h, \phi^e - \phi_h) \\
&\quad - [a_h(u^e, \phi^e - \phi_h) - ((f, \phi) - (f^e, \phi_h)_{\Gamma_h})] \\
&\quad - [a_h(u^e - u_h, \phi^e) - ((u, g) - (u_h, g^e)_{\Gamma_h})] \\
&= I_1 + I_2 + I_3 + I_4 + I_5.
\end{aligned}$$

We first estimate I_1. By applying the change of variable and the geometric error estimate (4.7), we have

$$|I_1| = ((1 - \mu_h)u^e, g^e)_{\Gamma_h} \lesssim h^2 \|u\|_{L^2(\Gamma_h)} \|g\|_{L^2(\Gamma_h)} \lesssim h^2 \|f\|_{L^2(\Gamma)} \|g\|_{L^2(\Gamma)}.$$

The estimation of I_2 is provided by the Lemma 4.10, from which we deduce

$$|I_2| \lesssim h^2 \|f\|_{L^2(\Gamma)} \|g\|_{L^2(\Gamma)}.$$

To estimate I_3, we apply the Cauchy–Schwartz inequality and the energy error estimates (4.38) and (4.43). Then, we obtain

$$|I_3| \lesssim \|u^e - u_h\|_h \|\phi^e - \phi_h\|_h \lesssim h^2 \|f\|_{L^2(\Gamma)} \|g\|_{L^2(\Gamma)}$$

According to Lemmas 4.11 and 4.5, we have

$$|I_4| + |I_5| \lesssim h^2 \|f\|_{L^2(\Gamma)} \|g\|_{L^2(\Gamma)}.$$

We complete the proof by combining all the above estimates. □

5 Superconvergent post-processing

In this section, we aim to generalize the parametric polynomial preserving recovery [26] to the surface Crouzeix–Raviart element.

The key idea of parametric polynomial preserving recovery is to take an intrinsic view on a surface. Instead of defining the surface gradient using tangential projection, we can compute the surface gradient in term of the metric tensor of the manifold. Let g denote the Riemann metric tensor of the manifold Γ. Then, the surface gradient is

$$\nabla_\Gamma u = \sum_{i,j} g^{ij} \partial_j u \partial_i, \tag{5.1}$$

where g^{ij} is the entry of the inverse of the metric tensor g, and ∂_i denotes the tangential basis.

In addition, a surface can be understood as a union of locally parametrized patches by Euclidean planar domains [25,35]. By introducing a local parametric mapping $\mathbf{r}$, we can map an open set in Euclidean space Ω_i to a port of the surface Γ_i as illustrated in Fig. 1. Once we are given a local parametric mapping, we can compute the metric tensor using the Jacobi matrix of $\mathbf{r}$. In specific, the surface gradient of u can be computed as

$$(\nabla_\Gamma u) \circ \mathbf{r} = \nabla \bar{u} (g \circ \mathbf{r})^{-1} \partial \mathbf{r}. \tag{5.2}$$

where $\bar{u} = u \circ \mathbf{r}$ is the pull back of the function u to the local planar parameter domain Γ, $\partial \mathbf{r}$ is the Jacobian of $\mathbf{r}$, and

$$g \circ \mathbf{r} = \partial \mathbf{r} (\partial \mathbf{r})^T. \tag{5.3}$$

Using the relation (5.3), we can rewrite (5.2) as

$$(\nabla_\Gamma u) \circ \mathbf{r} = \nabla \bar{u} (\partial \mathbf{r})^\dagger, \tag{5.4}$$

where $(\partial \mathbf{r})^\dagger$ denotes the Moore-Penrose inverse of $\partial \mathbf{r}$. For the definition of the surface gradient (5.2), [26] proved the following Lemma.

Lemma 5.1 *The gradient* (5.4) *is invariant using different local smooth bijective parametrization functions* $\mathbf{r}$.

Using the intrinsic definition of the surface gradient and its invariant property of the choice of isomorphic parametrization function $\mathbf{r}$, to reconstruct a better approximation of the surface gradient, we only need to reconstruct a better approximation of the pullback function $\bar{u}$ and the local parametric mapping $\mathbf{r}$. But those two functions are defined on the Euclidean domain Ω_i. It suggests us to use the gradient recovery techniques to reconstruct $\nabla \bar{u}$ and $\partial \mathbf{r}$. In this paper, we adopt the polynomial preserving recovery [38,49]. Our idea is to use a quadratic polynomial to approximate $\bar{u}$ and a vector of quadratic polynomials to $\mathbf{r}$. In other words, we use a quadratic polynomial to approximate $\bar{u}$ and use a quadratic polynomial surface to approximate the local

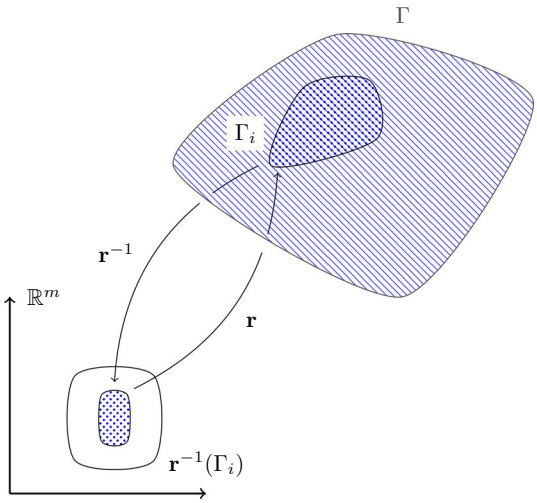

Fig. 1 Illustrate of the local parametric mapping

surface Γ_i. We achieve better approximations of $\nabla\bar{u}$ and $\partial\mathbf{r}$ by taking the gradient of the least-squares fitted polynomials.

Different from the linear surface element, the degrees of freedom of the surface Crouzeix–Raviart element are located on the edge midpoints of the approximate surface triangle instead of their vertices. We follow the idea of the gradient recovery method for the Crouzeix–Raviart element in [33] and define the gradient recovery operator $G_h : V_h \to V_h \times V_h$. Given a finite element function $u_h \in V_h$, we only need to define $(G_h u_h)(x_i)$ for all $x_i \in \mathcal{M}_h$.

For any $x_i = m_{E_i} \in \mathcal{M}_h$ and $n \in \mathbb{N}$, define the union of elements around x_i in the first n layers as follows

$$L(x_i, n) = \bigcup \{T : T \in \mathcal{T}_h \text{ and } T \cap L(x_i, n-1) \in \mathcal{E}_h\}, \tag{5.5}$$

with $L(x_i, 0) = \{E_i\}$. Let $L_i = L(x_i, n_i)$ with n_i being the smallest integer such that L_i satisfies the rank condition (see [49]) in the following sense:

Definition 5.1 The local element patch is said to satisfy the rank condition i if it admits a unique least-squares fitted polynomial in (5.6) and (5.7).

To recover the surface gradient at the given midpoint x_i, we firstly need construct a local parametric domain Ω_i. Lemma 5.1 says that we can choose arbitrary subdomain in an Euclidean space. In this paper, we firstly choose a vector ϕ_i^3 to be the normal vector of the local coordinate system. The main purpose of ϕ_i^3 is to help us to construct a local parametric domain. For the sake of simplicity, we choose $\phi_3^i = (n_{h_i}^+ + n_{h_i}^-)/2$. The local parameter domain Ω_i is selected to be orthogonal to ϕ_3^i and pass through x_i. Select x_i as the original of Ω_i and choose (ϕ_1^i, ϕ_2^i) as the tangent basis of Ω_i. We project all the midpoints in L_i onto the parameter domain Ω_i and the projections are denoted by ξ_j, for $j = 0, \ldots, n_i$.

Then, we reconstruct the local approximation surface S_i over Ω_i. As in [26], the approximate surface S_i can be approximated by the graph of a quadratic function on Ω_i. That is $S_i = \tilde{\mathbf{r}}_{h,i}(\Omega_i) = \cup_{\xi\in\Omega_i}(\xi, s_i(\xi))$, where

$$s_i = \arg\min_{s\in\mathbb{P}_2(\Omega_i)} \sum_{j=1}^{n_i} |s(\xi_j) - < x_{i_j}, \phi_3^i >|^2, \tag{5.6}$$

where $< \cdot, \cdot >$ means the Euclidean inner product in $\mathbb{R}^3$.

Our next step is to reconstruct a more accurate gradient for $\nabla\bar{u}_h$ on the parameter domain Ω_i. To do this, we use ξ_j as sampling points and fit a quadratic polynomial $p_i(\xi)$ over Ω_i in the least-squares sense

$$p_i = \arg\min_{p\in\mathbb{P}_2(\Omega_i)} \sum_{j=0}^{n_i} |p(\xi_j) - u_h(x_{i_j})|^2. \tag{5.7}$$

Calculate the partial derivatives of both the polynomial approximated surface function in (5.6) and the approximated polynomial function of surface FEM solution in (5.7), then we can approximate the tangential gradient which is given in (5.4) as

$$(G_h u_h)(x_i) = (\partial_1 p_i(0,0), \partial_2 p_i(0,0)) \begin{pmatrix} 1 & 0 & \partial_1 s_i(0,0) \\ 0 & 1 & \partial_2 s_i(0,0) \end{pmatrix}^{\dagger} (\phi_1^i, \phi_2^i, \phi_3^i)^T. \tag{5.8}$$

To multiply with the orthonormal basis $(\phi_1^i, \phi_2^i, \phi_3^i)$ is because we have to unify the coordinates from local ones to a global one.

Let $\{\chi_i(x)\}_{x_i\in\mathcal{M}_h}$ be the nodal basis functions of the surface Crouzeix–Raviart element. Then recovered gradient on the whole domain is

$$G_h u_h = \sum_{x_i\in\mathcal{M}_h} (G_h u_h)(x_i)\chi_{x_i}(x), \quad \forall x \in \Gamma_h. \tag{5.9}$$

As a direct application of the gradient recovery method, we naturally define a recovery-type a posteriori error estimator for the surface Crouzeix–Raviart element. The local a posteriori error estimator on each element T is defined as

$$\eta_{h,T} = \|G_h u_h - \nabla_{\Gamma_h} u_h\|_{L^2(T)}, \tag{5.10}$$

and the global error estimator as

$$\eta_h = \left(\sum_{T\in\mathcal{T}_h} \eta_{h,T}^2 \right)^{1/2}. \tag{5.11}$$

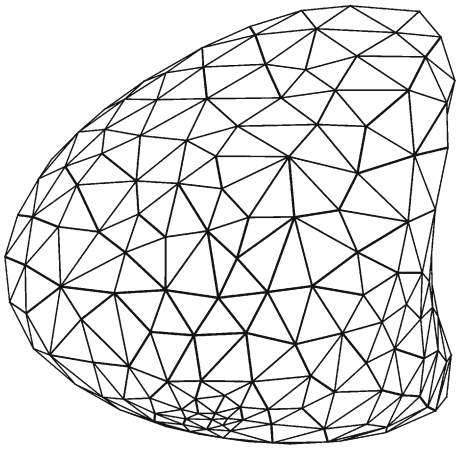

Fig. 2 Initial mesh for Dzuik surface

6 Numerical experiments

In this section, we present a series of benchmark numerical examples to validate the theoretical results and test the performance of the recovery-based a posteriori error estimator.

To generate an initial mesh on a general surface, we adopt the three-dimensional surface mesh generation module of the Computational Geometry Algorithms Library [45]. Meshes on finer levels are generated by firstly using uniform refinement for the first two numerical examples or the newest bisection [17] refinement for the other two numerical examples and then projecting them on to the surface.

For the sake of simplifying the notation, we introduce the following notation for errors

$$e := \|u^e - u_h\|_{L^2(\Gamma_h)}, \quad De := |u^e - u_h|_{H^1(\Gamma_h;\mathcal{T}_h)},$$
$$D_i e := \|\Pi_h u^e - u_h\|_{H^1(\Gamma_h;\mathcal{T}_h)}, \quad D_r e := \|\nabla u^e - G_h u_h\|_{L^2(\Gamma_h)}.$$

6.1 Numerical example 1

In this example, we consider the model problem (2.8) on a general surface firstly introduced by Dziuk [28]. Figure 2 shows the discretized surface and its initial mesh. The exact solution solution $u(x) = x_1 x_2$ and the right hand side function f can be computed from u.

We report the numerical results in Table 1. As predict by the Theorems 4.9 and 4.13, the L_2 error converges at a rate of $\mathcal{O}(h^2)$ and the discrete H^1 semi-error converges at a rate of $\mathcal{O}(h)$. Concerning the error between the finite element gradient and the gradient of the interpolation of the exact solution, $\mathcal{O}(h)$ convergence can be observed. It means that there is no supercloseness between the finite element gradient and the gradient of the interpolation of the exact solution, which is similar to the numerical results in planar

Table 1 Numerical results for numerical example 1

Dof	e	Order	De	Order	$D_i e$	Order	$D_r e$	Order
243	3.25e−02	–	7.02e−01	–	4.26e−01	–	3.61e−01	–
966	7.47e−03	2.13	3.69e−01	0.93	2.38e−01	0.84	1.20e−01	1.60
3858	1.86e−03	2.00	1.87e−01	0.98	1.24e−01	0.95	3.38e−02	1.83
15426	4.68e−04	1.99	9.37e−02	1.00	6.25e−02	0.99	9.05e−03	1.90
61698	1.17e−04	2.00	4.69e−02	1.00	3.13e−02	1.00	2.41e−03	1.91
246786	2.93e−05	2.00	2.35e−02	1.00	1.57e−02	1.00	6.57e−04	1.87

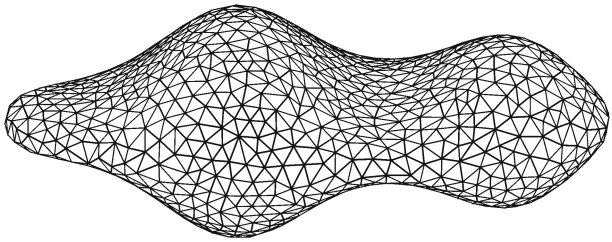

Fig. 3 Initial mesh for Elliot surface

Table 2 Numerical results for numerical example 2

Dof	e	Order	De	Order	$D_i e$	Order	$D_r e$	Order
1153	3.17e−02	–	7.39e−01	–	5.99e−01	–	4.31e−01	–
4606	8.32e−03	1.93	3.78e−01	0.97	3.18e−01	0.91	1.58e−01	1.45
18418	1.68e−03	2.31	1.86e−01	1.02	1.65e−01	0.94	4.63e−02	1.77
73666	4.40e−04	1.93	9.29e−02	1.00	8.37e−02	0.98	1.24e−02	1.90
294658	1.12e−04	1.97	4.64e−02	1.00	4.20e−02	1.00	3.26e−03	1.93
1178626	2.83e−05	1.99	2.32e−02	1.00	2.10e−02	1.00	8.64e−04	1.92
4714498	7.08e−06	2.00	1.16e−02	1.00	1.05e−02	1.00	2.35e−04	1.88

domain [33]. Even though in that case, we can observe $\mathcal{O}(h^{1.9})$ superconvergence for the recovered gradient.

6.2 Numerical example 2

Our second example to consider a general surface with high curvature part as in [26,29]. The discretized surface with the initial mesh was plotted in Fig. 3. We choose f to fit the exact solution $u(x) = x_1 x_2$.

In Table 2, we list the history of numerical errors. We can observe the same optimal convergence results in L^2 norm and discrete H^1 semi-norm which well match with the established theoretic results in Sect. 4. Similar to the previous example, $\mathcal{O}(h^{1.9})$ can be observed even though there is no supercloseness result.

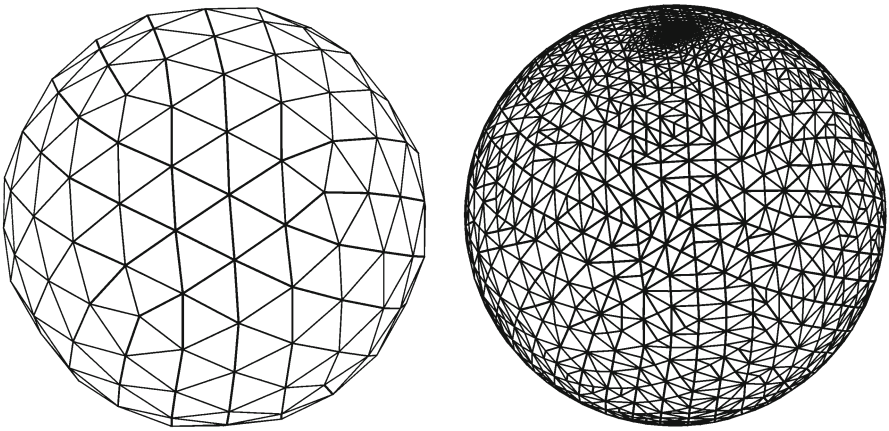

(a) **(b)**

Fig. 4 Meshes for numerical example 3: **a** initial mesh; **b** adaptively refined mesh

6.3 Numerical example 3

In all the previous numerical examples, the exact solutions are smooth. In this example, we consider a benchmark problem on the unit sphere surface with a singular solution. The solution and the source term in spherical coordinates are given by

$$u = \sin^{\lambda}(\theta)\sin(\phi), \quad f = (2+\lambda^2+\lambda)\sin^{\lambda}(\theta)\sin(\phi) + (1-\lambda^2)\sin^{\lambda-2}(\theta)\sin(\phi).$$

It is easy to show that $u \in H^{1+\lambda}(\Gamma)$. When $\lambda < 1$, the solution u has two singularities at north and south poles.

To resolve the singularity, we propose to apply the adaptive surface Crouzeix–Raviart element with the recovery based a posteriori error estimator (5.10). In this test, the initial mesh is chosen to be icosphere mesh as plotted in Fig. 4a. The bulk marking strategy [27] is also adopted. Figure 4b plots the resulting adaptive refined mesh after 14 adaptive refinements. It obvious that the refinement is mainly concentrated on the two singular points. We plot the errors in Fig. 5a. The L^2 error and discrete H^1 semi-error both converges optimally. The recovered gradient superconverges to the exact gradient at a rate of $\mathcal{O}(h^{1.5})$.

To quantify the performance of our new recovery-based *a posterior* error estimator (5.11) for the Laplace–Beltrami problem, the effectivity index κ is used to measure the quality of an error estimator [1,5], which is defined by the ratio between the estimated error and the exact error

$$\kappa = \frac{\|u_h - \nabla u_h\|_{L^2(\Gamma)}}{|u - u_h|_{H^1(\Gamma_h;\mathcal{T}_h)}} \tag{6.1}$$

The effectivity index is plotted in Fig. 5b. We see that κ converges asymptotically to 1 which indicates the posteriori error estimator (5.10) is asymptotically exact.

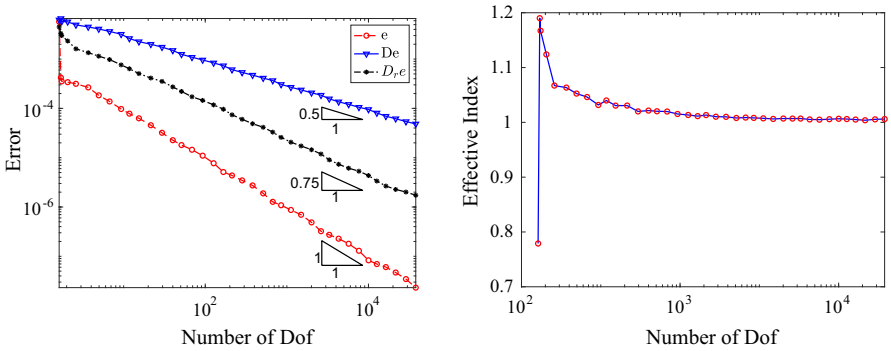

Fig. 5 Meshes for numerical example 3: **a** initial mesh; **b** adaptively refined mesh

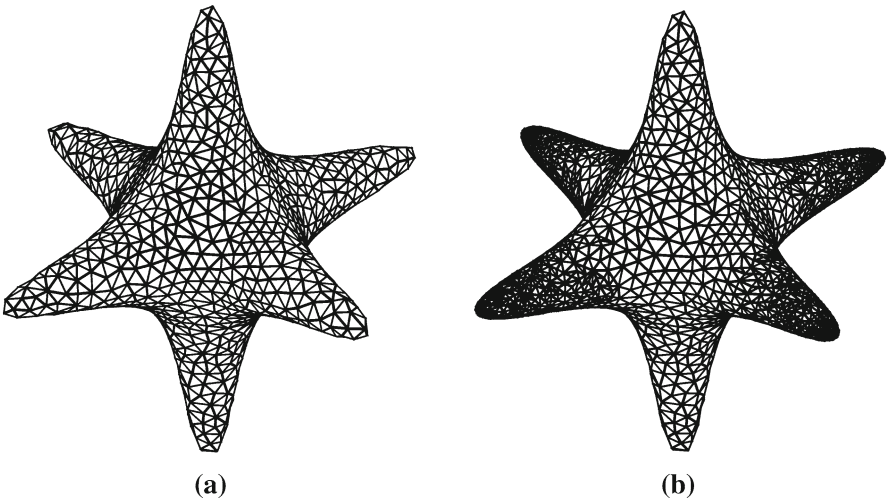

Fig. 6 Meshes for numerical example 4: **a** initial mesh; **b** adaptively refined mesh

6.4 Numerical example 4

This example is taken from [21]. The surface is the zero level of the following level set function

$$\phi(x) = 400(x_1^2x_2^2 + x_2^2x_3^2 + x_1^2x_3^2) - (1 - x_1^2 - x_2^2 - x_3^2)^3 - 40.$$

The discretized surface on the initial mesh is shown in Fig. 6a. What can be clearly seen in this figure is the the existence of the high curvature parts. The main numerical difficulties of this numerical example is that the initial mesh fails to resolve the high curvature feather of the surface. To capture the high curvature feature, our idea is to use the adaptive algorithms with the proposed recovery-based a posteriori error estimator

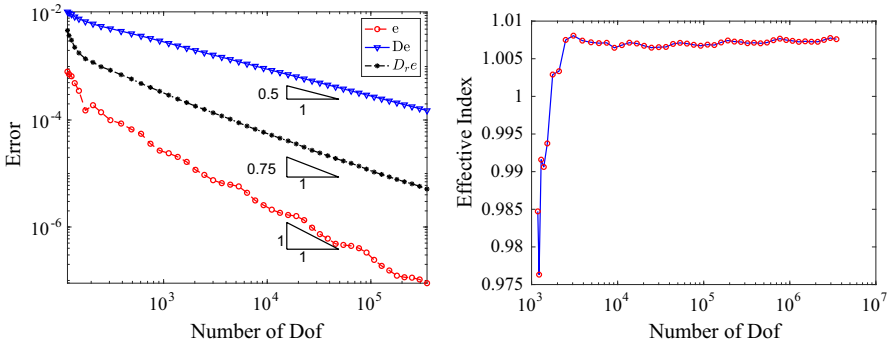

Fig. 7 Meshes for numerical example 4: **a** initial mesh; **b** adaptively refined mesh

(5.10). The adaptively refined mesh is plotted in Fig. 6b. It is clearly that the high curvature parts are well captured by the adaptively refined mesh.

Figure 7a plots the numerical errors in term of degrees of freedom. The figure shows the optimal decay of the L^2 error and discrete H^1 semi-error. In addition, we observe that the recovered gradient error superconverges at a rate of $\mathcal{O}(h^{1.5})$. In Fig. 7b, we graph the effectivity index κ. Figure 7b reveals that the effectivity index is close to 1 after several initial refinements. It illustrates that the recovery-type a posteriori error estimator (5.10) is asymptotically exact.

7 Conclusion

In this paper, we have introduced and analyzed the Crouzeix–Raviart element in a surface setting. The surface Crouzeix–Raviart element is considered to be a nonconforming element in the sense that it is only continuous at edge centers. In additional to the approximation error and the geometric error as in the standard continuous surface finite element method, there also exists a nonconforming consistency error caused by the discontinuity of the surface Crouzeix–Raviart element. Moreover, the nonconforming consistency error is typically coupled together with the geometric error. The standard argument for surface finite element method cannot be applied directly. We establish the optical convergence theory in both the discrete energy norm and L_2 norm by using a delicate argument in the discretized surface.

We also propose a superconvergent gradient recovery for the surface Crouzeix–Raviart element. The key idea of the post-processing algorithm is to take an intrinsic viewpoint of the surface gradient. The proposed surface gradient recovery method doesn't rely on any priori knowledge of the exact surface. The proposed post-processing procedure is numerical proven to be able to provide a more accurate approximate gradient and asymptotically exact a posteriori error estimator.

Ongoing research topics include using a residue-type a posterior error estimate to conduct medius error analysis [11] and applying it to investigate surface Stokes problems and surface Naiver–Stokes problems.

References

1. Ainsworth, M., Oden, J.T.: A Posteriori Error Estimation in Finite Element Analysis. Pure and Applied Mathematics (New York). Wiley-Interscience, New York (2000)
2. Antonietti, P.F., Dedner, A., Madhavan, P., Stangalino, S., Stinner, B., Verani, M.: High order discontinuous Galerkin methods for elliptic problems on surfaces. SIAM J. Numer. Anal. **53**, 1145–1171 (2015)
3. Arroyo, M., DeSimone, A.: Relaxation dynamics of fluid membranes. Phys. Rev. E **79**, 031915 (2009)
4. Aubin, T.: Best constants in the Sobolev imbedding theorem: the Yamabe problem. In: Seminar on Differential Geometry. Annals of Mathematics Studies, vol. 102, pp. 173–184. Princeton Univ. Press, Princeton (1982)
5. Babuška, I., Strouboulis, T.: The Finite Element Method and Its Reliability. Numerical Mathematics and Scientific Computation. The Clarendon Press, New York (2001)
6. Barrett, J.W., Garcke, H., Nürnberg, R.: Numerical computations of the dynamics of fluidic membranes and vesicles. Phys. Rev. E **92**, 052704 (2015)
7. Barrett, J.W., Garcke, H., Nürnberg, R.: A stable numerical method for the dynamics of fluidic membranes. Numerische Mathematik **134**, 783–822 (2016)
8. Bonito, A., Cascón, J.M., Mekchay, K., Morin, P., Nochetto, R.H.: High-order AFEM for the Laplace–Beltrami operator: convergence rates. Found. Comput. Math. **16**, 1473–1539 (2016)
9. Bonito, A., Cascón, J.M., Morin, P., Nochetto, R.H.: AFEM for geometric PDE: the Laplace-Beltrami operator. In: Brezzi, F., Colli Franzone, P., Gianazza, U., Gilardi, G. (eds.) Analysis and Numerics of Partial Differential Equations. Springer INdAM Series, vol. 4, pp. 257–306. Springer, Milan (2013)
10. Braess, D.: Finite Elements, 3rd edn. Cambridge University Press, Cambridge (2007). Theory, fast solvers, and applications in elasticity theory. Translated from the German by Larry L. Schumaker
11. Brenner, S.C.: Forty years of the Crouzeix–Raviart element. Numer. Methods Partial Differ. Equ. **31**, 367–396 (2015)
12. Brenner, S.C., Scott, L.R.: The Mathematical Theory of Finite Element Methods. Texts in Applied Mathematics, vol. 15, 3rd edn. Springer, New York (2008)
13. Brenner, S.C., Sung, L.-Y.: Linear finite element methods for planar linear elasticity. Math. Comput. **59**, 321–338 (1992)
14. Brezzi, F., Fortin, M.: Mixed and Hybrid Finite Element Methods. Springer Series in Computational Mathematics, vol. 15. Springer, New York (1991)
15. Burman, E., Hansbo, P., Larson, M.G., Larsson, K., Massing, A.: Finite element approximation of the Laplace-Beltrami operator on a surface with boundary. Numer. Math. **141**(1), 141–172 (2019)
16. Carstensen, C., Bartels, S.: Each averaging technique yields reliable a posteriori error control in FEM on unstructured grids. I. Low order conforming, nonconforming, and mixed FEM. Math. Comput. **71**, 945–969 (2002)
17. Chen, L.: Short implementation of bisection in MATLAB. In: Jorgensen, P., Shen, X., Shu, C.-W., Yan, N. (eds.) Recent Advances in Computational Sciences, pp. 318–332. World Sci. Publ, Hackensack (2008)
18. Ciarlet, P.G.: The Finite Element Method for Elliptic Problems. Classics in Applied Mathematics, vol. 40. Society for Industrial and Applied Mathematics (SIAM), Philadelphia (2002). Reprint of the 1978 original [North-Holland, Amsterdam; MR0520174 (58 #25001)]
19. Cockburn, B., Demlow, A.: Hybridizable discontinuous Galerkin and mixed finite element methods for elliptic problems on surfaces. Math. Comput. **85**, 2609–2638 (2016)
20. Crouzeix, M., Raviart, P.-A.: Conforming and nonconforming finite element methods for solving the stationary Stokes equations. I. Rev. Française Automat. Informat. Recherche Opérationnelle Sér. Rouge **7**, 33–75 (1973)
21. Dedner, A., Madhavan, P.: Adaptive discontinuous Galerkin methods on surfaces. Numer. Math. **132**, 369–398 (2016)
22. Dedner, A., Madhavan, P., Stinner, B.: Analysis of the discontinuous Galerkin method for elliptic problems on surfaces. IMA J. Numer. Anal. **33**, 952–973 (2013)
23. Demlow, A.: Higher-order finite element methods and pointwise error estimates for elliptic problems on surfaces. SIAM J. Numer. Anal. **47**, 805–827 (2009)
24. Demlow, A., Dziuk, G.: An adaptive finite element method for the Laplace–Beltrami operator on implicitly defined surfaces. SIAM J. Numer. Anal. **45**, 421–442 (2007). (**electronic**)

25. do Carmo, M.P.: Riemannian Geometry. Mathematics: Theory and Applications. Birkhäuser Boston, Inc., Boston (1992). Translated from the second Portuguese edition by Francis Flaherty
26. Dong, G., Guo, H.: Parametric polynomial preserving recovery on manifolds (2017). arXiv:1703.06509 [math.NA]
27. Dörfler, W.: A convergent adaptive algorithm for Poisson's equation. SIAM J. Numer. Anal. **33**, 1106–1124 (1996)
28. Dziuk, G.: Finite elements for the Beltrami operator on arbitrary surfaces. In: Partial Differential Equations and Calculus of Variations. Lecture Notes in Mathematics, vol. 1357, pp. 142–155. Springer, Berlin (1988)
29. Dziuk, G., Elliott, C.M.: Finite element methods for surface PDEs. Acta Numer. **22**, 289–396 (2013)
30. Elcott, S., Tong, Y., Kanso, E., Schröder, P., Desbrun, M.: Stable, circulation-preserving, simplicial fluids. ACM Trans. Graph. **26**, 4 (2007)
31. Fries, T.-P.: Higher-order surface fem for incompressible Navier–Stokes flows on manifolds. Int. J. Numer. Methods Fluids **88**, 55–78 (2018)
32. Grande, J., Reusken, A.: A higher order finite element method for partial differential equations on surfaces. SIAM J. Numer. Anal. **54**, 388–414 (2016)
33. Guo, H., Zhang, Z.: Gradient recovery for the Crouzeix–Raviart element. J. Sci. Comput. **64**, 456–476 (2015)
34. Larsson, K., Larson, M.G.: A continuous/discontinuous Galerkin method and a priori error estimates for the biharmonic problem on surfaces. Math. Comput. **86**, 2613–2649 (2017)
35. Lee, J.M.: Riemannian Manifolds. Graduate Texts in Mathematics, vol. 176. Springer, New York (1997). An introduction to curvature
36. Mekchay, K., Morin, P., Nochetto, R.H.: AFEM for the Laplace–Beltrami operator on graphs: design and conditional contraction property. Math. Comput. **80**, 625–648 (2011)
37. Mullen, P., Crane, K., Pavlov, D., Tong, Y., Desbrun, M.: Energy-preserving integrators for fluid animation. ACM Trans. Graph. **28**, 38:1–38:8 (2009)
38. Naga, A., Zhang, Z.: The polynomial-preserving recovery for higher order finite element methods in 2D and 3D. Discrete Contin. Dyn. Syst. Ser. B **5**, 769–798 (2005)
39. Olshanskii, M.A., Quaini, A., Reusken, A., Yushutin, V.: A finite element method for the surface stokes problem (2018). arXiv:1801.06589 [math.NA]
40. Olshanskii, M.A., Reusken, A., Grande, J.: A finite element method for elliptic equations on surfaces. SIAM J. Numer. Anal. **47**, 3339–3358 (2009)
41. Olshanskii, M.A., Safin, D.: A narrow-band unfitted finite element method for elliptic PDEs posed on surfaces. Math. Comput. **85**, 1549–1570 (2016)
42. Padberg-Gehle, K., Reuther, S., Praetorius, S., Voigt, A.: Transfer operator-based extraction of coherent features on surfaces. In: Carr, H., Garth, C., Weinkauf, T. (eds.) Topological Methods in Data Analysis and Visualization IV, pp. 283–297. Springer, Cham (2017)
43. Reusken, A.: Stream function formulation of surface stokes equations. IMA J. Numer. Anal. dry062 (2018) https://doi.org/10.1093/imanum/dry062
44. Reuther, S., Voigt, A.: Solving the incompressible surface Navier–Stokes equation by surface finite elements. Phys. Fluids **30**, 012107 (2018)
45. Rineau, L., Yvinec, M.: 3D surface mesh generation. In: CGAL User and Reference Manual, 4.9 ed. CGAL Editorial Board (2016)
46. Sasaki, E., Takehiro, S., Yamada, M.: Bifurcation structure of two-dimensional viscous zonal flows on a rotating sphere. J. Fluid Mech. **774**, 224–244 (2015)
47. Wei, H., Chen, L., Huang, Y.: Superconvergence and gradient recovery of linear finite elements for the Laplace–Beltrami operator on general surfaces. SIAM J. Numer. Anal. **48**, 1920–1943 (2010)
48. Wloka, J.: Partial Differential Equations. Cambridge University Press, Cambridge (1987). Translated from the German by C. B. Thomas and M. J. Thomas
49. Zhang, Z., Naga, A.: A new finite element gradient recovery method: superconvergence property. SIAM J. Sci. Comput. **26**, 1192–1213 (2005). (**electronic**)